Study of the structural, optical and electrical properties of PVA/SA performance by incorporating Al$_2$O$_3$ nanoparticles

M. Ibrahim[1] · K. M.A. Saron[1] · S. Ghalab[1] · G. M. Asnag[2] · M. A. Morsi[3,4] · A. E. Tarabiah[5]

Abstract

Aluminum oxide nanoparticles (Al$_2$O$_3$ NPs) were added to polyvinylpyrrolidone (PVP) and sodium alginate (SA) blend to synthesis nanocomposite films, using a solution casting technique, with favorable optical and electrical properties. The results reveal a series of noteworthy findings, where X-ray diffraction (XRD) measurement also shows that the addition of Al$_2$O$_3$ NPs to PVP/SA blend caused a decrease in the crystallinity of the filled samples. Fourier infrared (FTIR) analysis showed prominent characteristic peaks corresponding to vibrational groups characterizing the prepared nanocomposite samples, which change randomly with increasing concentration of Al$_2$O$_3$ NPs. Moreover, the indirect/direct optical energy gap decreased from 3.96/5.28 to 2.73/3.59 eV at 2.0 wt% of Al$_2$O$_3$ NPs, confirming the improvement in the optical features of the doped samples, as evidenced by UV/Vis spectra. After adding the nanoparticles to the blend, AC electrical conductivity increased and showed to follows Jonscher's rule. The maximum value of AC conductivity observed at 2.0 wt% of Al$_2$O$_3$ NPs in the blend is 1.445×10^{-6} S/cm. Additionally, the addition of the nanoparticles has been shown to increase in dielectric loss and dielectric constant of the composite samples. The improvement of the optical and electrical properties due to filling with Al$_2$O$_3$ NPs indicates the possibility of using the prepared nanocomposites in optoelectronic devices. Also, studying the effect of incorporating Al$_2$O$_3$ nanoparticles into PVP/SA blends has attracted little attention in the literature; therefore, this study is considered as a new research one.

1 Introduction

Nanomaterials play a vital role in the industrial revolution, enabling the production of advanced, efficient and energy-efficient devices. They are particularly useful in the conversion and storage of renewable energy, such as lithium-ion batteries, fuel cells, solar thermal systems, and lighting. Understanding their optical and electronic properties is essential for the next generation of optoelectronic devices. Metal oxide nanoparticles, such as aluminum

---

Extended author information available on the last page of the article

oxide nanoparticles (Al_2O_3 NPs), are in high demand due to their superior optical, mechanical, electrical and chemical features. Al_2O_3 NPs are suggested for use in a number of industries, such as ceramic manufacture, lubricating liquids, adsorbents, catalysts, lubricating concrete mixtures, microelectronics, cosmetics, and textiles (Gudkov et al. 2022).

Polymer-based nanocomposites have been fabricated by incorporating nanofillers and plasticizers into the host polymeric matrix in order to enhance electrical conductivity. Currently, polymer/nano batteries can be considered an essential energy source due to their amazing properties (Kumar and Rao 2019; Abdali et al. 2023). Polymer-based nanocomposites and/or polymer blends have been proposed as a very attractive approach to harnessing Al_2O_3 nanoparticle benefits in the near future. Among these polymers, Polyvinylpyrrolidone (PVP) and Sodium Alginate (SA) are interesting polymers with excellent electrical, optical and mechanical properties. Sodium alginate is a natural hydrophilic polymer produced from brown marine algae with excellent electrical, optical, and mechanical properties. SA polymer is frequently used in biotechnology and industrial applications such as electronic component production, coating, food packaging, texturing and paper processing (Farea et al. 2022a, b). SA can be cross linked with various polymers and inorganic fillers due to the presence of (-OH) and -COOH groups in its polymeric matrix. PVP is an extremely thermally stable, highly viscous, non-toxic, pH-stable, biodegradable, and biocompatible material that can be used in a range of biomedical applications (Awasthi et al. 2018; Zein et al. 2022). Carbonyl groups (C=O) on PVP's side chains allow it to form complexes with a diverse of inorganic ions (Ravi et al. 2013). It can be blended with sodium alginate to improve the thermal and mechanical features of the blend (Zia et al. 2017; Caykara et al. 2007). It is therefore not surprising that researchers are keen to investigate the physical and chemical characteristics of PVP/SA filled blends. A PVP/SA/Au nanocomposite was studied under gamma radiation by Farea et al. (Kumar and Rao 2019). The values of AC conductivity and dielectric parameters of PVP/NaAlg blend were improved as a result of the incorporation of Au NPs and gamma irradiation, as these values depend largely on the irradiation dose. El Gohary et al. (El Gohary et al. 2023) prepared PVA/SA/Ag-TiO_2 nanocomposites, where the increase in the AC conductivity of the doped samples was assigned to an increase in both the mobile charges carriers of the nanoparticles as well as the amorphousity ratio of the polymeric samples. Hence, these properties made Ag-TiO_2 nanoparticles preferred candidates for enhancing the thermal and antimicrobial activity of PVA/SA blend. For bone repair and wound dressings, Fadeeva et al. (Fadeeva et al. 2021), studied PVP/SA/Hydroxyapatite hydrogel composites. Dhatarwal and Sengwa (Dhatarwal and Sengwa 2021) studied the optical properties of PVP/PVA/Al_2O_3 nanocomposites. It was observed that the values of direct/indirect bandgaps and optical permittivity gradually increased with increasing content of Al_2O_3 in PVP/PVA blend. Devikala et al. (Devikala et al. 2019) reported the addition of Al_2O_3 on the electrical and dielectric properties of PVA, finding that the dielectric and AC conductivity of the polymeric samples increased with increasing Al_2O_3 concentrations and temperature. The prepared samples were suitable for various technological uses. In this present work, we present an accessible and cost-effective method to prepare electrolytic nanocomposites. Using the solution casting technique, PVP and SA were combined with Al_2O_3 nanoparticles in this work to form elastic, lightweight nanocomposite materials with improved optical and electrical/dielectric features. A variety of methods and procedures are employed to investigate the structural, electrical, optical, and dielectric characteristics of

these samples. Notably, these nanocomposites provide customizable optical, electrical and dielectric properties, making them suitable for a wide range of applications.

2 Experimental details

2.1 Chemicals used

SA with M.W. of 100,000 g/mol and PVP with M.W. of 233,000 g/mol were acquired from Sigma, Aldrich, Germany and BDH, U.K., respectively. Aluminum Oxide (Al_2O_3), CAS#: 1344-28-1, Product Number: NG02MD0102, Nanopowder/Nanoparticles Dispersion in Water Gamma, Size: 8 nm, 22 wt%, were purchased from Nanografi Nanotechnology. As a solvent, tetrahydrofuran (THF) was used.

2.2 Preparation of PVP/SA/Al_2O_3 NPs nanocomposites

A quantity of SA and PVP polymers (50/50 wt%) were dissolved in tetrahydrofuran (THF) at 50 °C separately. Then, the two solutions of the blend components were combined and stirred continuously for three hours (at 500 rpm) to obtain a homogenous mixture. Al_2O_3 NPs were then added to PVP/SA blend solution at different weight ratios (0.00, 0.25, 0.50, 1.00 and 2.00 wt% of Al_2O_3 NPs) with continuous stirring until the desired viscosity was achieved. In order to produce nanocomposite films, the viscous solutions were placed into properly cleaned Petri dishes, and dried for two days at 40 °C. The nanocomposites were removed from the dishes after drying, and then stored in vacuum desiccator. These films ranged in thickness from 0.004 to 0.006 cm.

2.3 Measurements

Measurement of the X-ray diffraction analysis was obtained using a PANalytical XPert PRO XRD at 30 kV with Bragg angle ranging from 5° to 70°. TEM image of Al_2O_3 NPs was conducted using a JEOL-JEM-1011 at 200 kV. Fourier transform infrared (FTIR) spectra of PVP/SA/Al_2O_3 nanocomposites were obtained by Nicolet iS10 FTIR spectroscopy between 4000–400 cm^{-1}. UV/visible spectra were obtained via JASCO V-630-Japan at wavelengths between 190 and 800 nm. Electrical and impedance characteristics of the nanocomposite samples were measured via broadband dielectric spectroscopy equipment (Novo Control Turnkey Concept/40 equipment) at frequencies range from 10^{-1} to 2×10^7 Hz at room temperature.

3 Results and discussion

3.1 XRD and TEM measurements

Figure 1 illustrates XRD patterns of Al_2O_3 NPs and PVP/SA polymer blends containing various concentrations of Al_2O_3 NPs. XRD scan of pure Al_2O_3 nanoparticles identified distinct peaks at 33, 37.4, 39.8, 45.9, 61.1, 67.2 representing the (220), (311), (222), (400), (422),

and (440) planes, respectively. Based on the JCPDS card number 79-1558, these Al_2O_3 NPs have a cubic phase (Alkallas et al. 2022). Using Scherer's relation (Salim and Tarabiah 2023), the crystallite size (L) for Al_2O_3 NPs can be calculated from:

$$L = (0.9\lambda / \beta \cos\theta) \qquad (1)$$

Where β indecates the width at half-maximum (FHWM) of the relevant XRD peak and λ stands for the applied wavelengths. Using the above relation, the obtained average size for an Al_2O_3 particle size is L = 14 nm.

The scan of pure PVP/SA blend showed broad peaks at 2θ = 22.14 and 33.57, indicating that the blend has an amorphous structure, as shown in Fig. 1. Moreover, the Figure shows that the peaks intensity of PVP/SA blend decreases after filling, whereas the peaks of the Al_2O_3 NPs appeared and increased with increasing concentration. In other words, Al_2O_3 NPs crystallinity is increases at the expense of PVP/SA composite matrix. Fillers' interactions with polymer blends are believed to reduce intermolecular interactions between polymer chains and also reduce crystallinity of the blend matrix, which causes the PVP/SA peak to decrease as Al_2O_3 NPs increase. Al_2O_3 NPs have been shown to provide better ionic mobility and conductivity of the nanocomposites matrix through this optimization of the amorphous structure (Mohamed et al. 2022). Many polymeric Al_2O_3 nanocomposites have similar behaviours (Mohamed et al. 2022; Choudhary 2018; Rai et al. 2022).

Figures < link rid="fig2">2</link>-a and 2-b demonstrate TEM image and histogram distribution map of Al_2O_3 NPs. Based on these Figures; we can conclude that Al_2O_3 NPs have an irregularly distributed, almost spherical, and crystalline with a crystal diameter between 2 and 15 nm, with an average diameter of 7 nm (Gudkov et al. 2022; Alkallas et al. 2022; Mohamed et al. 2022).

3.2 FTIR measurement

Figure 3 provides FTIR spectra of composite PVP/SA doped with different Al_2O_3 NPs content. There are distinct vibration peaks of bending and stretching in the resulting spectrum of the functional group in the produced films.

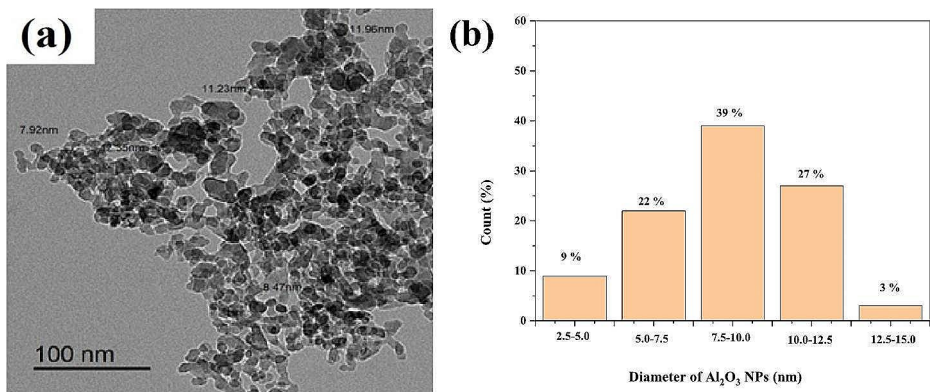**Fig. 1** XRD scans of pure Al_2O_3 nanoparticles and SA/PVP/Al_2O_3 nanocomposite samples
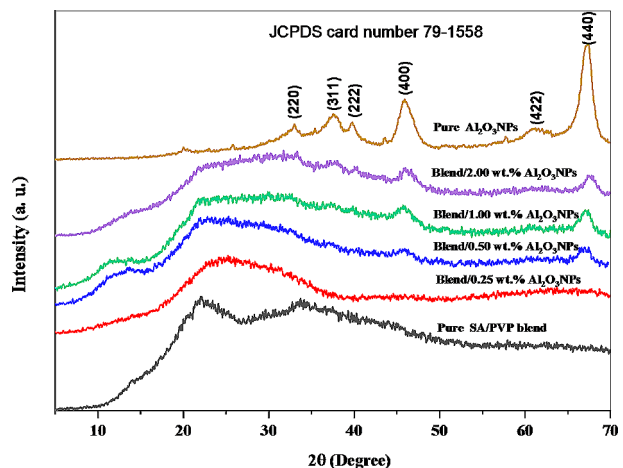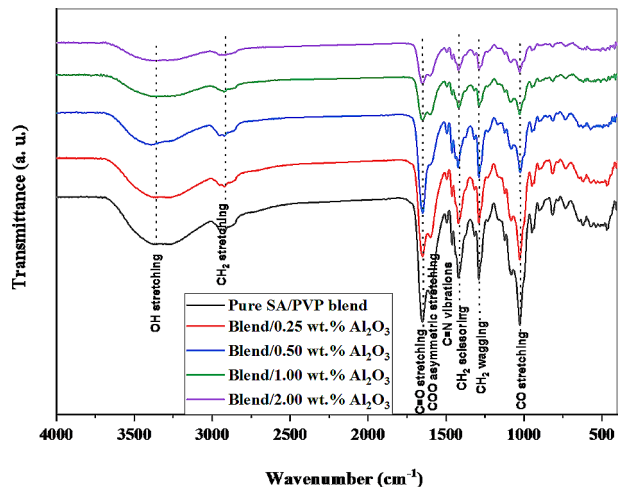
Fig. 2 (**a**) TEM image and (**b**) the histogram of size distribution of Al_2O_3 NPs.

Fig. 3 FTIR transmittance spectra of SA/PVP/Al_2O_3 nanocomposite samples

Pure blend spectrum show large distinctive absorption bands for PVP at 1651 cm^{-1} form C=O stretching, 1420 cm^{-1} of CH_2 scissoring, and 1289 cm^{-1} form CH_2 wagging (Waly et al. 2022; Zidan et al. 2019). The large characteristic peaks of SA are 1600 cm^{-1} form COO asymmetric stretching, 1081 and 1027 cm^{-1} from CO stretching (El-Mohdy 2017; Badita et al. 2020). Further band assignments are provided in Table 1 derived from FTIR spectrum of the pure blend. After filling with Al_2O_3 NPs, these absorption peaks decreased gradually with increasing Al_2O_3 NPs content. Moreover, small peaks in the range of 417–601 cm^{-1} appeared after filling with Al_2O_3 NPs, which is consistent with vibrations of O-Al-O in Al_2O_3 NPs (Dhawale et al. 2019). These obtained data support the PVP/SA blend's interplay and complexation with Al_2O_3 NPs because of the high miscibility of Al_2O_3 NPs with the blend used in this study. In addition, the existence of double bonds within the system makes

Table 1 FTIR transmittance peaks and their assignments of the pure sample

| Wavenumber (cm^{-1})	Bands assignment	Sources	Ref.
3314	OH stretching	PVP+SA	(Waly et al. 2022), (El-Mohdy 2017; Nomier et al. 2022)
2951, 2921	CH_2 stretching	PVP+SA	(Waly et al. 2022), (Nomier et al. 2022)
1651	C=O stretching	PVP	(Waly et al. 2022)
1600	COO asymmetric stretching	SA	(Badita et al. 2020)
1494	C=N (pyridine ring) vibrations	PVP	(Zidan et al. 2019)
1461	CH bending of CH_2 and/or OH bending	PVP	(Waly et al. 2022)
1420	CH_2 scissoring	PVP	(Zidan et al. 2019)
1382	CH_2 bending	PVP	(Waly et al. 2022)
1289	CH_2 wagging	PVP	(Waly et al. 2022)
1231	C-C stretching and/or CH_2 deformation	PVP	(Waly et al. 2022)
1123	C–O–C stretching	SA	(Chen et al. 2021)
1081, 1027	CO stretching	SA	(El-Mohdy 2017)
947	Uronic acid	SA	(Nomier et al. 2022)
900	CH_2 bending	PVP	(Waly et al. 2022)
815	Mannuronic acid	SA	(Nomier et al. 2022)
733	CH_2 rocking	PVP	(Waly et al. 2022)
642	CN bending	PVP	(Waly et al. 2022)
417, 450, 475, 508, 601	Al-O stretching	Al_2O_3	(Dhawale et al. 2019)

them suitable site for polarons and/or bipolarons. These sites can operate as hopping sites for charges carriers (Tawansi et al. 1997).

3.3 UV/visible measurement

Figure 4 shows UV/visible absorbance spectra for PVP/SA blends filled with varying Al_2O_3 NPs content. For pure PVP/SA, a high intensity peak is observed at 210 nm. This peak could represent n→π* transitions due to carbonyl groups in the blend structure (Mohamad et al. 2019; Aziza et al. 2019). After filling, this peak gradually shifts to the longer wavelength side with increasing content of Al_2O_3 NPs. This shift indicates changes in the band gap energies of SA/PVP/Al_2O_3 nanocomposites, which may have been a result of complexation and interaction between Al_2O_3 NPs and the PVP/SA blend. Generally, it was observed that absorbance decreases with increasing wavelengths of incident photons, and tends toward constant values at high wavelengths part (Badita et al. 2020).

The expression for absorption depends on the absorption coefficient (α), which represents the relative rate at which the intensity of incident light decreases per unit length of the medium (Mohamad et al. 2019; Aziza et al. 2019). The Beer Lambert equation was used to calculate α at the equivalent frequency from the absorbance spectra (A) (Dhawale et al. 2019):

Fig. 4 UV-vis. absorbance spectra of SA/PVP/Al_2O_3 nanocomposite samples
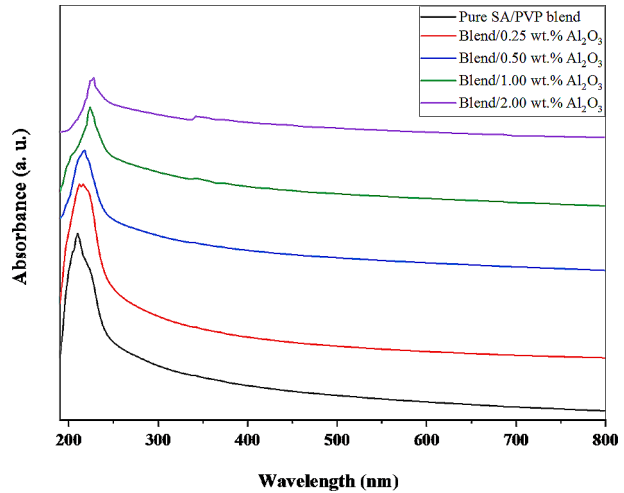
Where, the incident and transmitted light intensities are represented by I_o and I, respectively, and d is the sample thickness. The value of the optical absorption coefficient can be used to indicate the type of electronic transition responsible for photons absorption within the polymeric matrix (Mohamad et al. 2019). Also, using Tuac's equation (Salim and Tarabiah 2023), the direct/indirect optical bandgap E_g for PVP/SA/Al_2O_3 nanocomposite samples can be obtained as:

$$\alpha = \frac{2.303}{d}\log\frac{I_o}{I} = \frac{2.303}{d}A \tag{2}$$

$$\alpha = \frac{B(h\upsilon - E_g)^r}{h\upsilon} \tag{3}$$

Where B represents a constant that depends upon the probability that an electronic transition will take place and hυ represents the energy of the incident photon. Power r refers to the type of transitions occurring in k-space. Power r can have various values of 0.5, 1.5, 2.0 and 3.0, which correspond to the direct allowed, direct forbidden, indirect allowed and indirect bandgap transitions, respectively (Salim and Tarabiah 2023; Mohamad et al. 2019; Aziza et al. 2019). Figure 5(a, b, c) illustrate the variation of $(\alpha h\upsilon)^{1/2}$, $(\alpha h\upsilon)^2$ and (α) vs. hυ, showing the values of indirect bandgap $(E_g^{Ind.})$ and direct optical $(E_g^{Dir.})$ bandgap and absorption edge (E_e) for existing nanocomposites. The variations in the Ee values for the PNC samples indicate that there were interactions between the polymeric chains and Al_2O_3 nanoribbons (Mohamad et al. 2019; Aziza et al. 2019). The values of direct bandgap, indirect bandgap and absorption edge and AC conductivity were compared with previous studies and are summarized in Table 2. According to the results, the optical bandgap energies decrease with the increasing Al_2O_3 NPs content. In other words, Al_2O_3 NPs may play a role in altering the electronic structure of PVP/SA blend sample due to the emergence of different levels of polaronics and defects. Al_2O_3 NPs and defect concentrations are related to intensity of the localized states N(E) (Abdelghany et al. 2019; Al-Muntaser et al. 2020). Increasing Al_2O_3 NPs content can lead to the localized states of different colour centres to stretch in the hop-
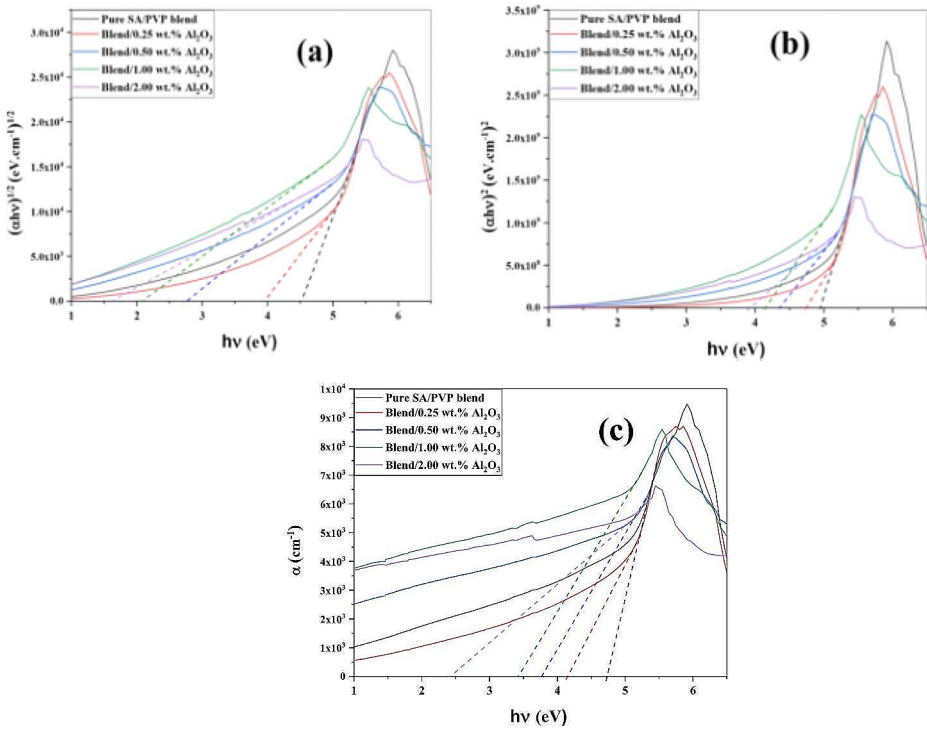
Fig. 5 (**a**) $(\alpha h\upsilon)^{0.5}$, (**b**) $(\alpha h\upsilon)^2$ and (α) vs. of photons energy (hυ) for SA/PVP blend loaded with various concentration of Al_2O_3 NPs.

ping gap. As a result of this overlap, the energy gaps may decrease (Al-Muntaser et al. 2020; Abdali 2023; El-Naggar et al. 2023). These results indicate that the filled films may be suitable for optoelectronic and electrochemical applications. The same results were observed in spectrum analyses of PVP/SA blend films loaded with gold NPs (Abdelghany et al. 2019) and also PVC/PMMA loaded with $Li_4Ti_5O_{12}$ NPs (Al-Muntaser et al. 2020).

3.4 Conductivity studies

Amorphous polymeric composites exhibit frequency-dependent conductivity due to the increased mobility of charge carriers within their matrix. Current amplitude and phase (relative to the applied voltage) are monitored by applying a sinusoidal voltage to the samples. Based on the signal frequency f, AC conductivity is calculated as follows:

$$\sigma_{ac} = \omega \varepsilon' \varepsilon_0 \tan \delta \qquad (4)$$

Where ω is the angular frequencies ($\omega = 2\pi \times f$), $tan\delta$ refers to dissipation factor, ε' and ε_o are dielectric constants of the materials and free space.

Table 2 The direct bandgap, indirect bandgap and absorption edge values and AC conductivity (σ_{ac}) of the present SA/PVP/Al$_2$O$_3$ nanocomposites and different polymeric samples from the literature survey:

Samples	$E_g^{Ind.}$ (eV)	$E_g^{Dir.}$ (eV)	E_e (eV)	σ_{ac} (S/cm)	References
Pure SA/PVP blend	4.50	4.95	4.74	1.35×10^{-7}	Present samples
SA/PVP/0.25 wt% Al$_2$O$_3$ NPs	3.97	4.73	4.16	2.45×10^{-7}	Present samples
SA/PVP/0.50 wt% Al$_2$O$_3$ NPs	2.75	4.35	3.77	3.80×10^{-7}	Present samples
SA/PVP/1.00 wt% Al$_2$O$_3$ NPs	2.07	4.14	3.41	5.71×10^{-7}	Present samples
SA/PVP/2.00 wt% Al$_2$O$_3$ NPs	1.64	3.92	2.43	1.445×10^{-6}	Present samples
Pure MC	5.85	6.25	5.85	----	27
MC/0.30 wt% Pbs	1.35	1.92	1.35	----	27
Pure PMMA	4.80	5.03	----	----	28
PMMA+30 mL CNDs	4.00	4.20	----	-----	28
Pure PVA/CMC blend	3.97	4.79	----	5.01×10^{-7}	33
PVA/CMC/1.6 wt% Cu/Se NPs	2.39	3.59	----	6.76×10^{-6}	33
Pure PVP/CMC blend	4.76	5.15	----	5.12×10^{-6}	36
PVP/CMC/MWCNTs/1.00 wt% Ag NPs	0.65	3.04	----	1.74×10^{-8}	36

Fig. 6 The variation of Log (σ_{ac}) with Log f for PVP/SA blend loaded with different contents Al$_2$O$_3$ NPs.
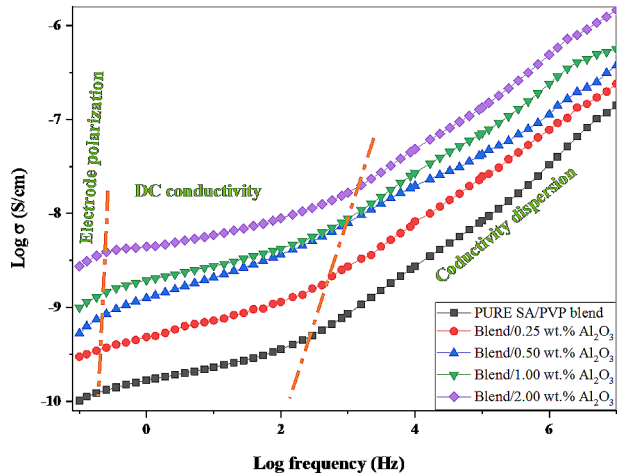
Figure 6 shows the change in the electrical conductivity of studied composites with frequency. The results demonstrate that the conductivity of the samples increased with increasing Al$_2$O$_3$ NPs concentration. As Al$_2$O$_3$ NPs concentration increases, the conductive pathways are increased within PVP/SA structure. It is known that the shape, size, type, and dispersion of nanocomposites added to polymeric composites are all factors that affect its electrical conductivity (Abdallah et al. 2023; Rahaman et al. 2017). Additionally, the

amorphous nature of the polymer blend may have contributed to increased conductivity since it lowers the energy barrier, allowing ions to move more easily through it (Abdelrazek et al. 2019). The figure also shows that electrical conductivity increases with increasing frequency. It is shown in three regions: (i) The low-*f* dispersion region has σ' levels are low resulting from the electrode polarization effect (Morsi et al. 2023). (ii) The Mid-*f* region is linked to the DC conductivity σ_{dc} and associated with the bulk conductivity of the sample, caused by the displacement of charge carriers (Rahaman et al. 2017). (iii) The high-*f* dispersion region has a linear relationship between frequency and conductivity, since charge carriers move easier at high frequencies than at low frequencies (Hemalatha et al. 2015). The σ' values in high and mid-*f* regions follow the power law of dispersion as in the following relation (Abdelrazek et al. 2019; Farea et al. 2022a, b):

$$\sigma_{ac}(\omega) = \sigma_{dc} + A\omega^s \tag{5}$$

Where *s* is an exponent with values between 0 and 1 depending on temperature and frequency, *A* is a temperature-dependent component that influences the degree of polarization, and σ_{dc} is D.C. conductivity ($\omega=0$) (Al-Muntaser et al. 2022a, b). It has also been observed that increasing the content of Al_2O_3 NPs causes the high frequency dispersion region to be shifted towards a higher frequency region. These behaviors are called the "universal dynamic response" (UDR), according to Jonscher, and are common for many other nanocomposites (Salim and Tarabiah 2023; Abdelrazek et al. 2019; Al-Muntaser et al. 2022a, b).

3.5 The complex dielectric (ε*)

The dielectric constant (**ε′**) and dielectric loss (**ε″**) are the real and imaginary parts of the complex dielectric (ε*). The dielectric constant indicates the material's ability to store charge, whereas the dielectric loss indicates how much charge is dissipated from that material. In higher frequencies part or energy applications, lower dielectric constant values are used to reduce electrical energy losses. For capacitive applications requiring small sizes, high dielectric constant values are recommended (Campo 2008). The dielectric constants and loss values are calculated from

$$\epsilon' = \frac{Cd}{\epsilon_0 A}$$

$$\epsilon'' = \frac{\sigma}{\omega \epsilon_0} \tag{7}$$

(6)

Where d, A, and C are the sample thickness, cross-sectional area, and capacitance, respectively.

As shown in Fig. 7, ε′ and ε″ are changed with frequency for the studied PVP/SA/Al_2O_3 nanocomposites. As the frequency increases, ε′ and ε″ decline significantly until they become minor values. High ε′ and ε″ values at low frequencies may be caused by electrode effects as well as interface effects, which dominate large parts of the sample. Furthermore, it is believed that the initial values of ε′ and ε″ for polar materials are high, but as the field frequencies increase, their values decrease. Further, polar materials' initial values of ε′ and ε″ are believed to be high, but their values decrease as the field frequency increases as the
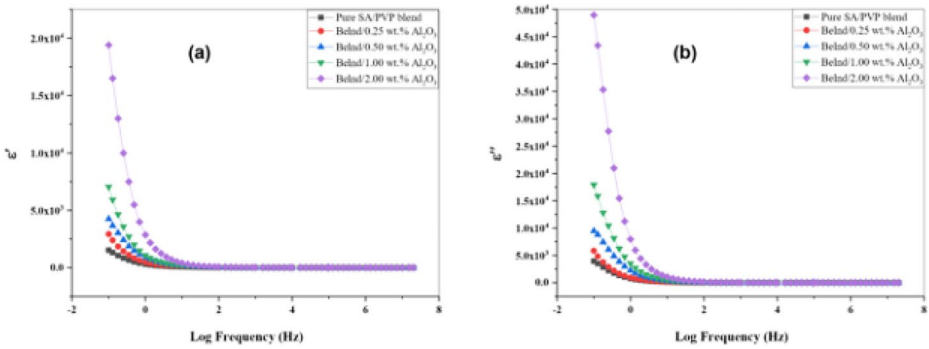
Fig. 7 The variation of: (**a**) dielectric constant ε′ and (**b**) dielectric loss ε″ with Log (f) for PVP/SA blend loaded with different contents Al$_2$O$_3$ nanoparticles

dipoles can't keep up with field fluctuations (Salim et al. 2022; Abdelrazek et al. 2022). . After filling with Al$_2$O$_3$ NPs, all frequency ranges showed an increase in ε′ and ε″ values. Within the insulating matrix, Al$_2$O$_3$ NPs are like nanocapacitors (Islam et al. 2022). As the concentration of Al$_2$O$_3$ NPs increases, these nanocapacitors become more prevalent, resulting in a higher net capacitance (i.e., dielectric constant). It has also been reported that nanofillers reduce the limitations on the dipole's response to the applied electric fields, resulting in greater dielectric constants (Thakur et al. 2017).

3.6 Complex electric modulus (M*)

Dielectric parameters, such as complex electric modulus (M*) and complex impedance (Z*), are investigated to interpret dielectric spectra (Jonscher 1999). When capacitive and/or resistive analysis is dominated by localized relaxation, M* formula is preferable; but, when long-range conduction dominates, Z* formula is preferred. The complex electric modulus is calculated using the next relation:

$$M^* = \frac{1}{\epsilon} = \frac{\epsilon'}{\left(\epsilon'\right)^2 + \left(\epsilon''\right)^2} + \frac{i\epsilon''}{\left(\epsilon'\right)^2 + \left(\epsilon''\right)^2} = M' + iM'' \tag{8}$$

Where M′, M″ represent the real and imaginary components of M*, respectively.

Figure 8 shows the differences between M′ and M″ with Log (f) for the studied samples. A step-like transition is seen in M′, suggesting that samples have an inherently high capacitance, as shown in Fig. 8a. In addition, increasing the Al$_2$O$_3$ NPs concentration led to a decrease in M′, suggesting that the actual component of the dielectric constant rises with increasing filler content (Yu et al. 2000; Patsidis and Psarras 2008; Alawi and Al-Bermany 2023). In Fig. 8b, the M″ curves demonstrate a wide relaxation peak that decreases with increasing Al$_2$O$_3$ NP content. With increasing filler concentration, this peak also shifts slightly toward higher frequencies. The existence of relaxation peaks reveals that these materials may be ionic conductors (Langar et al. 2017). The asymmetric nature and wide M″ peaks of the curve are explained by the distribution of relaxation times and deviations from the ideal behavior of the Debye type (Isasi et al. 1995). Further, the range of frequencies below the M″max peak is associated with DC conductivity caused by continuous charge
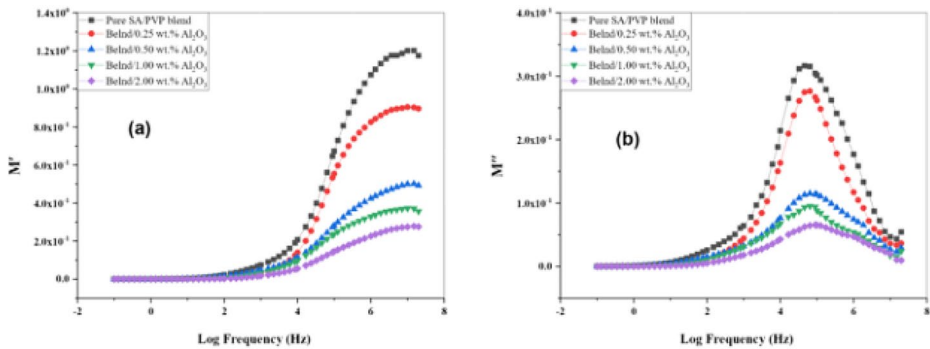
Fig. 8 The variation of: (**a**) real (M′) and (**b**) imaginary (M″) parts of electric modulus with Log (f) for PVP/SA blend loaded with different contents Al₂O₃ NPs.

carriers hopping over long distances. As a result, the range of frequencies above the M″max corresponds to relaxation polarization, and represents a frequency range during which ions are spatially confined within their potential wells, and can only move within these wells for a short distance (Isasi et al. 1995; El-Falaky et al. 2012). Since ions move reversibly over a limited area, the right side of the peak is representative of AC conductivity. Thus, an increase in frequency indicates a change in mobility from long to short ranges.

3.7 Complex impedance (Z^*)

The investigated samples can be undergo to complex impedance analysis according to the following (Khalil 2017):

$$Z^* = Z' - iZ'' = \frac{1}{i\omega\epsilon_o\epsilon^*} \tag{9}$$

Where Z′ and Z″ are the real and imaginary component of Z^*, respectively. Figure 9-a provides the Nyquist curves for the studied samples at ambient temperature over a wide frequencies range from 10^{-1} to 2×10^7 Hz. Each Nyquist curve has an inclined spike at low frequencies and a depressed semicircle arc at high frequencies. Together, the inclined spike and semicircle demonstrate the usual behaviour of conductive ionic samples. The inclined spike results from the migration of low-frequency ions creation of two layers of capacitance at the interfaces of the electrode/electrolyte. Bulk resistance (produced by ions' movement) and bulk capacitance (produced by immobile polymeric chains) are combined in a semi-circular arc (Farea et al. 2022a, b). Semi-circular arcs have depressions at their centre due to non-Debye ionic relaxation mechanisms. The abnormal thickness and morphology of the studied films and/or the roughness of electrode surfaces may cause this deviation from Debye type (Lanfredi et al. 2002).

Additionally, as Al₂O₃ NPs concentration increases, the diameter of the semicircle shrinks, resulting in a decrease in bulk resistivity and an increase in ionic conductivity. Impedance data are expressed as equivalent circuits with resistances and capacitances in order to establish a relationship between electrical properties and microstructure. Figure 9.b illustrates an equivalent circuit that was created from the collected impedance measurements
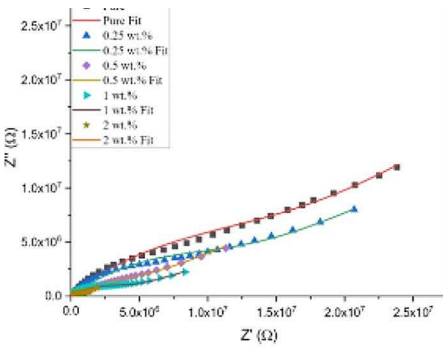
(a)
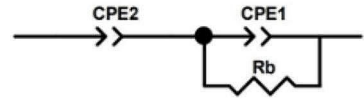
(b)

Fig. 9 (**a**) Nyquist plot for the examined films, (**b**) related equivalent circuit elements

Table 3 Equivalent circuit fitting parameters

sample	Fitting parameters				
	Rb (Ω)	Q_1(F)	n_1	Q_2(F)	n_2
SA/PVP	1.41×10^7	1.81×10^{-8}	0.55	8.00×10^{-8}	0.47
SA/PVP – 0.25 wt% Al_2O_3	9.46×10^6	1.25×10^{-8}	0.54	8.50×10^{-8}	0.36
SA/PVP – 0.50 wt% Al_2O_3	4.20×10^6	3.10×10^{-8}	0.43	1.36×10^{-7}	0.34
SA/PVP – 1.00 wt% Al_2O_3	3.00×10^6	1.15×10^{-8}	0.48	1.94×10^{-7}	0.25
SA/PVP – 2.00 wt% Al_2O_3	1.00×10^6	9.00×10^{-8}	0.52	9.00×10^{-7}	0.40

using EIS software. In this circuit, bulk resistance R_b is combined with partial capacitance CPE in parallel. CPE impedance can be determined by applying the following formula:

$$Z_{CPE} = 1/Q(i)^n \tag{10}$$

This relationship indicates how far the capacitor deviates from purity, where Q is the scalar value of $|Z|^{-1}$ at $= 1$ rad/s, and n is the element's phases. When n=zero, it behaves like a pure resistor, while when $n=1$, the CPE behaves like a pure capacitor.

Based on the curves in Fig. 9.a, Table 3 summarizes the equivalent circuit model's parameters. With increasing concentrations of Al_2O_3 NPs, the bulk resistance R_b decreases, indicating that there are more conductive channels connected (Nasrallah et al. 2021). In addition to increasing the number of charge carriers, the decrease in the crystallinity level of the samples may be responsible for the decrease in R_b. Furthermore, bulk capacitance values (Q) rise with increasing Al_2O_3 NPs concentration, which is consistent with the prior description of many nano-capacitors being produced (Islam et al. 2022). There is a high level of correlation between the observations and the modelling results, suggesting that the equivalent circuit was chosen in a realistic manner and that the PVP/SA/Al_2O_3 NPs samples prepared are likely to be suitable for high-power lithium-polymer batteries.

4 Conclusion

By solution casting, nanocomposite films of PVP/SA blended with different Al_2O_3 NPs contents were produced. Al_2O_3 NPs were found to have a cubic phase with sizes ranging between 2 and 15 nm based on XRD and TEM analyses. X-ray study shows that Al_2O_3 NPs have grown crystallinity at the expense of PVP/SA blend matrix. FTIR spectra of the nanocomposites revealed that the vibrational peaks changed randomly after the addition of Al_2O_3 nanoparticles. In the nanocomposite matrix, polarons and/or bipolarons may be responsible for the charge carrier hopping, as indicated by the double bond assigned to C=O and C=N. UV/Vis absorbance spectrum of pure PVP/SA sample showed a 210 nm peak that may be caused by n→π* transitions. In addition, there was a decrease in the optical bandgaps of the nanocomposite samples based on the concentration of Al_2O_3 NPs. The complexity and interactions between the blend and Al_2O_3 NPs were revealed by XRD, UV/visible, and FTIR analyses. According to the impedance spectroscopy analysis, an increase in the concentration of Al_2O_3 NP improved AC electrical conductivity of the nanocomposite at room temperature. The equivalent electrical circuits of the films were determined by analyzing their impedance components Z′ and Z″. PVP/SA/Al_2O_3 nanocomposite samples possess outstanding electrical and optical characteristics that make them ideal for optoelectronic applications.

Author contributions M. I: Conceptualization; Data curation; Writing original draft.K.M.A S: Formal analysis Validation; Visualization.S. G: Investigation; MethodologyG.M. A: Review & editingM.A. M: Validation; Writing - review and editingA. T: Formal analysis Validation; VisualizationAll authors reviewed the manuscript.

Declarations

Competing interests The authors declare no competing interests.

References

Abdali, K.: Novel flexible Glass Composite Film for Stretchable devices Applications. Silicon. **15**, 5187–5195 (2023)

Abdali, K., Rabee, B.H., Al-Bermany, E., Abdulridha, A.R., Abass, K.H., Kadim, A.M.: Effect of Doping Sb_2O_3NPs on Morphological, Mechanical, and Dielectric properties of PVA/PVP Blend Film for Electromechanical Applications. Nano. **18**(03), 2350011 (2023)

Abdallah, E.M., Asnag, G.M., Morsi, M.A., Aljohani, M., Albalwa, A.N., Yassin, A.Y.: Elucidation of the Effect of Hybrid copper/selenium Nanofiller on the Optical, Thermal, Electrical, Mechanical Properties and Antibacterial Activity of Polyvinyl alcohol/carboxymethyl Cellulose Blend. Polymer Engineering & Science (2023)

Abdelghany, A., Oraby, A., Farea, M.: Influence of green synthesized gold nanoparticles on the structural, optical, electrical and dielectric properties of (PVP/SA) blend. Phys. B: Condens. Matter. **560**, 162–173 (2019)

Abdelrazek, E.M., Abdelghany, A.M., Tarabiah, A.E., Zidan, H.M.: AC conductivity and dielectric characteristics of PVA/PVP nanocomposite filled with MWCNTs. J. Mater. Sci.: Mater. Electron. **30**, 15521–15533 (2019)

Abdelrazek, E.M., Abdelghany, A.M., Tarabiah, A.E., Waly, A.L.: Mechanical and electrical studies of PVA/PVP blend filled with MWCNTs. Polym. Bull. 1–14. (2022)

Al-Muntaser, A., Abdelghany, A., Abdelrazek, E., Elshahawy, A.: Enhancement of optical and electrical properties of PVC/PMMA blend films doped with Li4Ti5O12 nanoparticles. J. Mater. Res. Technol. **9**, 789–797 (2020)

Al-Muntaser, A., AlSaidi, R.A., Sharma, K., Alamri, H.R., Makhlouf, M.: Structural, optical, electrical, and DFT studies on polyvinyl pyrrolidone/polyethylene oxide polymer blend filled with MoO3 nanoplates for flexible energy-storage devices. Int. J. Energy Res. **46**, 13832–13843 (2022a)

Al-Muntaser, A.A., Pashameah, R.A., Sharma, K., Alzahrani, E., Tarabiah, A.E.: Reinforcement of structural, optical, electrical, and dielectric characteristics of CMC/PVA based on GNP/ZnO hybrid nanofiller: Nanocomposites materials for energy-storage applications. Int. J. Energy Res. **46**, 23984–23995 (2022b)

Alawi, A.I., Al-Bermany, E.: Newly fabricated Ternary PAAm-PVA-PVP Blend Polymer Doped by SiO$_2$: Absorption and dielectric characteristics for solar cell applications and antibacterial activity, **15** 5773–5789. (2023)

Alkallas, F.H., Ahmed, H.A., Alrebdi, T.A., Pashameah, R.A., Alrefaee, S.H., Alsubhe, E., Trabelsi, A.B.G., Mostafa, A.M., Mwafy, E.A.: Removal of Ni (II) ions by poly (vinyl alcohol)/Al2O3 Nanocomposite Film via laser ablation in Liquid. Membranes. **12**, 660 (2022)

Awasthi, R., Manchanda, S., Das, P., Velu, V., Malipeddi, H., Pabreja, K., Pinto, T.D.J.A., Gupta, G., Dua, K.: 9 - Poly(vinylpyrrolidone), in: A. Parambath (Ed.), Engineering of Biomaterials for Drug Delivery Systems, Woodhead Publishing pp. 255–272. (2018)

Aziza, S.B., Abdullaha, O.G., Brza, M.A., Azawy, A.K., Tahir, D.A.: Effect of carbon nano-dots (CNDs) on structural and optical properties of PMMA polymer composite. Results Phys. **15**, 102776 (2019)

Badita, C., Aranghel, D., Burducea, C., Mereuta, P.: Characterization of sodium alginate based films. Rom J. Phys. **65**, 1–8 (2020)

Campo, E.A.: 4 - Electrical properties of Polymeric materials. In: Campo, E.A. (ed.) Selection of Polymeric Materials, pp. 141–173. William Andrew Publishing, Norwich, NY (2008)

Caykara, T., Demirci, S., Kantoğlu, Ö.: Thermal, spectroscopic, and mechanical properties of blend films of poly (n-vinyl-2-pyrrolidone) and sodium alginate. Polym.-Plast. Technol. Eng. **46**, 737–741 (2007)

Chen, J., Wu, A., Yang, M., Ge, Y., Pristijono, P., Li, J., Xu, B., Mi, H.: Characterization of sodium alginate-based films incorporated with thymol for fresh-cut apple packaging. Food Control. **126**, 108063 (2021)

Choudhary, S.: Structural, morphological, thermal, dielectric, and electrical properties of alumina nanoparticles filled PVA–PVP blend matrix-based polymer nanocomposites. Polym. Compos. **39**, E1788–E1799 (2018)

Devikala, S., Kamaraj, P., Arthanareeswari, M.: AC conductivity studies of PVA/Al$_2$O$_3$ composites, Materials Today: Proceedings 14 288–295. (2019)

Dhatarwal, P., Sengwa, R.J.: Investigation on the optical properties of (PVP/PVA)/Al$_2$O$_3$ nanocomposite films for green disposable optoelectronics. Phys. B. **613**, 412989 (2021)

Dhawale, V.P., Late, D.J., Kulkarni, S.D.: Synthesis, characterization of α-Al 2 O 3 nanoparticles and its application in decolorization of Methyl Orange Azo Dye in the Presence of UV light. J. Nanosci. Technol. **580**, 583 (2019)

El Gohary, H.G., Alhagri, I.A., Qahtan, T.F., Al-Hakimi, A.N., Saeed, A., Abolaban, F., Alshammari, E.M., Asnag, G.M.: Reinforcement of structural, thermal and electrical properties and antibacterial activity of PVA/SA blend filled with hybrid nanoparticles (ag and TiO$_2$ NPs): Nanodielectric for energy storage and food packaging industries. Ceram. Int. **49**, 20174–20184 (2023)

El-Falaky, G.E., Guirguis, O.W., Abd El-Aal, N.S.: Conductivity and relaxation dynamics in zinc–borate glasses. Progress Nat. Science: Mater. Int. **22**, 86–93 (2012)

El-Mohdy, H.A.: Radiation-induced degradation of sodium alginate and its plant growth promotion effect. Arab. J. Chem. **10**, S431–S438 (2017)

El-Naggar, A.M., Brnawi, S.Z., Kamal, A.M., Albassam, A.A., Heiba, Z.K., Mohamed, M.B.: Structural, optical, and Electrical Parameters of Doped PVA/PVP blend with TPAI or THAI salt. Polymers. **1512**, 2661 (2023)

Fadeeva, I.V., Trofimchuk, E.S., Forysenkova, A.A., Ahmed, A.I., Gnezdilov, O.I., Davydova, G.A., Kozlova, S.G., Antoniac, A., Rau, J.V.: Composite Polyvinylpyrrolidone–Sodium Alginate—Hydroxyapatite Hydrogel films for bone repair and wound dressings applications. Polymers. **13**, 3989 (2021)

Farea, M., Pashameah, R.A., Sharma, K., Alzahrani, E., Al-Muntaser, A., Sugair, M.T., Morsi, M.: Gamma irradiation boosted the optical and electrical properties of PVP/NaAlg/Au ternary nanocomposite films for flexible optoelectronic devices. Polym. Bull. 1–21. (2022a)

Farea, M.O., Pashameah, R.A., Sharma, K., Alzahrani, E., Al-Muntaser, A.A., Sugair, M.T.S., Morsi, M.A.: Gamma irradiation boosted the optical and electrical properties of PVP/NaAlg/Au ternary nanocomposite films for flexible optoelectronic devices. Polym. Bull. 1–21. (2022b)

Gudkov, S.V., Burmistrov, D.E., Smirnova, V.V., Semenova, A.A., Lisitsyn, A.B.: A Mini Review of Antibacterial properties of Al2O3 nanoparticles. Nanomaterials. **12**, 2635 (2022)

Hemalatha, K., Sriprakash, G., Ambika Prasad, M., Damle, R., Rukmani, K.: Temperature dependent dielectric and conductivity studies of polyvinyl alcohol-ZnO nanocomposite films by impedance spectroscopy. J. Appl. Phys. **118**, 154103 (2015)

Isasi, J., López, M.L., Veiga, M.L., Ruiz-Hitzky, E., Pico, C.: Structural characterization and Electrical properties of a Novel defect pyrochlore. J. Solid State Chem. **116**, 290–295 (1995)

Islam, M., Rahaman, M., Aldalbahi, A., Paikaray, B., Moharana, J., Mondal, S., Das, N.C., Gupta, P., Giri, R.: High density polyethylene and metal oxides based nanocomposites for high voltage cable application. J. Appl. Polym. Sci. **139**, 51787 (2022)

Jonscher, A.K.: Dielectric relaxation in solids. J. Phys. D **32**, R57 (1999)

Khalil, R.: Impedance and modulus spectroscopy of poly(vinyl alcohol)-Mg[ClO4]2 salt hybrid films. Appl. Phys. A. **123**, 422 (2017)

Kumar, M.S., Rao, M.C.: Effect of Al_2O_3 on structural and dielectric properties of PVP-CH$_3$COONa based solid polymer electrolyte films for energy storage devices. Heliyon. **5**, e02727 (2019)

Lanfredi, S., Saia, P.S., Lebullenger, R., Hernandes, A.C.: Electric conductivity and relaxation in fluoride, fluorophosphate and phosphate glasses: Analysis by impedance spectroscopy. Solid State Ionics. **146**, 329–339 (2002)

Langar, A., Sdiri, N., Elhouichet, H., Ferid, M.: Structure and electrical characterization of ZnO-Ag phosphate glasses. Results Phys. **7**, 1022–1029 (2017)

Mohamad, A.H., Saeed, S.R., Abdullah, O.G.: Synthesis of very-fine PbS nanoparticles dispersed homogeneously in MC matrix: Effect of concentration on the structural and optical properties of host polymer. Mater. Res. Express. **6**, 115332 (2019)

Mohamed, H.F., Abdel-Hady, E.E., Abdel-Moneim, M.M., Bakr, M.A., Soliman, M.A., Shehata, M.G., Ismail, M.A.: Effect of Al2O3 on nanostructure and ion transport properties of PVA/PEG/SSA polymer electrolyte membrane. Polymers. **14**, 4029 (2022)

Morsi, M., Pashameah, R.A., Sharma, K., Alzahrani, E., Farea, M., Al-Muntaser, A.: Hybrid MWCNTs/Ag nanofiller reinforced PVP/CMC blend-based polymer nanocomposites for multifunctional optoelectronic and nanodielectric applications. J. Polym. Environ. **31**, 664–676 (2023)

Nasrallah, D.A., El-Metwally, E.G., Ismail, A.M.: Structural, thermal, and dielectric properties of porous PVDF/Li4Ti5O12 nanocomposite membranes for high-power lithium-polymer batteries. Polym. Adv. Technol. **32**, 1214–1229 (2021)

Nomier, Y.A., Alshahrani, S., Elsabahy, M., Asaad, G.F., Hassan, A.: El-Dakroury, ameliorative effect of chitosan nanoparticles against carbon tetrachloride-induced nephrotoxicity in Wistar rats. Pharm. Biol. **60**, 2134–2144 (2022)

Patsidis, A., Psarras, G.C.: Dielectric behaviour and functionality of polymer matrix–ceramic BaTiO$_3$ composites, currents 5 (2008)

Rahaman, M., Aldalbahi, A., Govindasami, P., Khanam, N.P., Bhandari, S., Feng, P., Altalhi, T.: A new insight in determining the percolation threshold of electrical conductivity for extrinsically conducting polymer composites through different sigmoidal models. Polymers. **9**, 527 (2017)

Rai, N., Singh, C.P., Ranjta, L.: Structural, thermal and electrical studies of Al2O3 nanoparticle soaked electrolyte gel films for novel proton conducting (H+ion) eco-friendly device applications. Am. J. Nano Res. Appl. **10**, 1–8 (2022)

Ravi, M., Bhavani, S., Kumar, K.K., Rao, V.N.: Investigations on electrical properties of PVP: KIO4 polymer electrolyte films. Solid State Sci. **19**, 85–93 (2013)

Salim, E., Tarabiah, A.: The influence of NiO nanoparticles on Structural, Optical and Dielectric properties of CMC/PVA/PEDOT: PSS nanocomposites. J. Inorg. Organomet. Polym Mater. 1–8. (2023)

Salim, E., Hany, W., Elshahawy, A., Oraby, A.: Investigation on optical, structural and electrical properties of solid-state polymer nanocomposites electrolyte incorporated with ag nanoparticles. Sci. Rep. **12**, 1–13 (2022)

Tawansi, A., Zidan, H., Moustafa, Y., Eldumiaty, A.: Optical and electrical properties of NiCl2 filled PVC films. Phys. Scr. **55**, 243 (1997)

Thakur, Y., Zhang, T., Iacob, C., Yang, T., Bernholc, J., Chen, L.Q., Runt, J., Zhang, Q.M.: Enhancement of the dielectric response in polymer nanocomposites with low dielectric constant fillers. Nanoscale. **9**, 10992–10997 (2017)

Waly, A., Abdelghany, A., Tarabiah, A.: A comparison of silver nanoparticles made by green chemistry and femtosecond laser ablation and injected into a PVP/PVA/chitosan Polymer blend. J. Mater. Sci.: Mater. Electron. **33**, 23174–23186 (2022)

Yu, S., Hing, P., Hu, X.: Dielectric properties of polystyrene–aluminum-nitride composites. J. Appl. Phys. **88**, 398 (2000)

Zein, R., Alghoraibi, I., Soukkarieh, C., Ismail, M.T., Alahmad, A.: Influence of polyvinylpyrrolidone concentration on properties and anti-bacterial activity of green synthesized silver nanoparticles. Micromachines. **13**, 777 (2022)

Zia, K.M., Zuber, M., Muhammad, A.: Algae Based Polymers, Blends, and Composites: Chemistry, Biotechnology and Materials Science. Elsevier Science (2017)

Zidan, H.M., Abdelrazek, E.M., Abdelghany, A.M., Tarabiah, A.E.: Characterization and some physical studies of PVA/PVP filled with MWCNTs. J. Mater. Res. Technol. **8**, 904–913 (2019)

Authors and Affiliations

M. Ibrahim[1] · K. M.A. Saron[1] · S. Ghalab[1] · G. M. Asnag[2] · M. A. Morsi[3,4] · A. E. Tarabiah[5]

✉ M. Ibrahim
momibrahim@ju.edu.sa

[1] Physics Department, College of Science and Arts, Jouf University, P.O. Box: 756, Al-Gurayyat, Saudi Arabia

[2] Department of Mechatronics, College of Engineering and Information Technology, Emirates International University, Sana'a 16881, Yemen

[3] Physics Department, Faculty of Science, Taibah University, Al-Ula, Medina, Saudi Arabia

[4] Mathematical and Natural Sciences Department, Faculty of Engineering, Egyptian Russian University, Badr City 11829, Cairo, Egypt

[5] Dental Biomaterials Department, Faculty of Oral and Dental Medicine, Delta University for Science and Technology, Gamasa 35712, Egypt